*modelling*

MDPI

*Article*

# Impact of Volute Throat Area and Gap Width on the Hydraulic Performance of Low-Specific-Speed Centrifugal Pump

**Muhammad Fasahat Khan [1,*], Tim Gjernes [2], Nicholas Guenther [2] and Jean-Pierre Hickey [1]**

[1] Department of Mechanical and Mechatronics Engineering, University of Waterloo, 200 University Avenue West, Waterloo, ON N2L 3G1, Canada; jean-pierre.hickey@uwaterloo.ca
[2] Toyo Pumps North America Corp, 1550 Brigantine Dr, Coquitlam, BC V3K 7C1, Canada; tgjernes@toyopumps.com (T.G.); nguenther@toyopumps.com (N.G.)
* Correspondence: mf9khan@uwaterloo.ca

**Abstract:** This paper investigates the influence of the volute geometry on the hydraulic performance of a low-specific-speed centrifugal pump using numerical simulations. The performance characteristics for the pump with the volute geometry designed using the constant velocity method show a significant discrepancy between the design point and the best efficiency point (BEP). This design methodology also results in a relatively flat head–capacity curve. These are both undesirable characteristics which can be mitigated by a reduction in the volute throat area. This design methodology also leads to a reduction in the power consumption and an increase in efficiency, especially at underload and design flow conditions. These impacts of the volute throat area on performance characteristics are investigated in terms of the change in internal flow characteristics due to the reduction in the volute throat area. Another aspect of the study is the impact of the width of the volute gap on performance characteristics. A reduction in the gap width results in a nearly vertical shift of the head–capacity curve, so that head delivered is higher across all the flow rates as the gap width is reduced. This is also accompanied by a slight improvement in efficiency under design flow and overload conditions. Numerical simulations are used to relate the change in performance characteristics with internal flow characteristics.

**Keywords:** centrifugal pumps; low specific speed; volute throat area; volute gap width



**Citation:** Khan, M.F.; Gjernes, T.; Guenther, N.; Hickey, J.-P. Impact of Volute Throat Area and Gap Width on the Hydraulic Performance of Low-Specific-Speed Centrifugal Pump. *Modelling* **2024**, *5*, 659–672. https://doi.org/10.3390/modelling5030035

Academic Editor: Sergey Utyuzhnikov

Received: 5 May 2024
Revised: 21 June 2024
Accepted: 23 June 2024
Published: 26 June 2024



## 1. Introduction

Centrifugal pumps have applications in a wide range of industries, such as water and wastewater treatment plants, petroleum, oil and gas industries, space propulsion, and other energy systems. Centrifugal pumps are known for their robustness, with fewer parts that can be worn out compared to alternatives such as piston pumps; this is a particularly relevant characteristic for handling particle-laden, multi-phase flows such as slurries. Hence, centrifugal pumps tend to have a longer life and reduced material costs because fewer operating parts are required. They are designed for a wide range of flow rates and head outputs, thus they find applications in many aspects of industry [1], with a total global production of greater than USD 20 billion per year [1]. An important design parameter used for pumps is the specific speed:

$$n_q = \frac{n\sqrt{Q_{opt}}}{H_{opt}^{0.75}} \quad (1)$$

It is defined in terms of the head required, $H_{opt}$, in meters, at the specified rotor speed, $n$, in revolutions per minute (rpm) and flow rate, $Q_{opt}$, in $m^3/s$. Generally, a centrifugal pump is considered to have low specific speed if $n_q < 20$ [1]. These pumps are of particular importance, especially in the petrochemical industry and in space technology, where the pumps operate at a higher rotor speed and lower flow rate than those used in the normal

specific speed range [2]. However, low-specific-speed centrifugal pumps suffer from a number of performance problems. One such issue is the instability in the head–capacity curve; the stability criterion is violated if the slope of the head–capacity curve is positive $dH/dQ > 0$. Low-specific-speed centrifugal pumps also suffer from disk friction losses that increase as the specific speed decreases. Increased disk friction losses result in reduced hydraulic efficiency. This problem can be overcome by reducing the diameter of the impeller, since disk friction is proportional to the fifth power of the diameter [1]. However, a diameter reduction comes at the cost of a lower head delivery. Therefore, the diameter of the impeller is often a limiting factor in the design of low-specific-speed centrifugal pumps.

In addition to reduced efficiency, the best efficiency point (BEP) of low-specific-speed pumps has been found to have a much higher discharge rate than that corresponding to the design point [3]. Ideally, the BEP should be near the design point. These performance issues have inspired unconventional designs for low-specific-speed applications. Perhaps, the first investigation into the topic of low-specific-speed centrifugal pumps was carried out by Barske [4,5], who proposed a semi-open impeller with radial vanes as a favorable impeller design for low-specific-speed hydraulics. Dahl showed that this impeller design delivered a higher head compared to that of a conventionally designed impeller throughout the operating range [5]. This impeller design has a higher blade outlet angle of 90° and allows a larger number of blades to be used. Both of these factors contribute to the higher head delivered. A semi-open impeller has the additional advantage of reduced disk friction losses. However, with a semi-open impeller, an additional parameter, the tip clearance ratio, becomes significant. Performance characteristics improve as the tip clearance decreases and worsen as the clearance increases [3,6]. This effect is more pronounced for pumps in the low-specific-speed range [6]. However, if the tip clearance is too small, there is a danger of seizure through contact, which will severely affect pump performance. Furthermore, experimental evidence has shown the presence of strong leakage/secondary flow through the tip clearance of the low-specific-speed centrifugal pump that negatively affects performance characteristics [3].

Other unconventional designs have been proposed for low-specific-speed applications. Satoh et al. [7] proposed a palm-sized pump whose impeller was designed as a disk with ditches engraved across the radius that functioned as flow passages. The design was shown to have satisfactory performance. Another pump design, proposed by Kagawa et al. [8], involved a disk with many J-shaped shallow grooves on either side, similar to the design proposed by Barske, which was shown to have stable head–capacity characteristics and higher head output than that delivered by a conventionally designed impeller. Olimstad et al. [9] used experimental investigations to iterate on several impeller designs for low-specific-speed applications and proposed an impeller design with S-shaped blades that produced better performance features than other design options. Other similar unconventional design options for low-specific-speed pumps have been investigated.

There have also been parametric studies investigating the impact of different design variables on the performance characteristics of low-specific-speed pumps. Cui et al. [10] used experimental and numerical investigations to conclude that a higher blade outlet angle results in greater static and total pressure at the impeller outlet at the design flow rate, while also improving the efficiency. Gao et al. [11] used numerical simulations to study the impact of different trailing edge profiles of impeller blades on the performance. Their results showed that elliptical profiles result in higher efficiency, while also reducing the amplitude of pressure pulsations at the impeller–volute interface. Balasubramanian et al. [12] examined the impact of the different blade leading edge profiles on the cavitation performance, concluding that parabolic profiles, of all the profiles examined, led to the least cavitation, while the blunt leading edge profile led to the most cavitation within the pump. Recently, Li [13] investigated the impact of different interface models on the accuracy of numerical simulations through comparison of the results produced from numerical simulations for each interface model with experimental data. The study concluded that an interface model

and the impeller domain used for simulations can have a noticeable impact on the accuracy of the simulations.

Recently, there have been studies aimed at coupling different optimization algorithms with numerical simulations to iterate over the design space of the variables that define the geometry of the pump to identify the design that optimizes an objective function of concern. Chen and Yuan [14] developed an optimization strategy for turbomachinery blade design by parameterizing the blade geometry using B-spline curves. The blade designs resulted in higher efficiency for all the turbomachinery types tested. An et al. [15] developed a framework utilizing an evolutionary genetic algorithm to optimize the impeller design for reduced cavitation and improved hydraulic efficiency at the design point. The optimized design resulted in diminishing secondary flow phenomenon within the impeller passage, which improved the efficiency of the pump. Donno et al. [16] developed a surrogate-based optimization technique to optimize the parameterized pump geometry at the operating condition. The optimized pump had its efficiency raised by 3% with reduced power consumption. Lin et al. [17] used a surrogate model based on the Particle Swarm Optimization algorithm and least square support vector regression to optimize the geometry of a multi-stage centrifugal pump for head delivery and efficiency. The refined pump geometry had its efficiency raised at almost all the flow rates considered with reduced energy losses.

Although most of the emphasis is placed on the impeller design for centrifugal pumps, the volute can also play a significant role in impacting the performance characteristics. Kurokawa et al. [18] suggested that optimization of volute parameters can have a positive influence on the performance of low-specific-speed centrifugal pumps. Enlargement of the volute throat area has been shown to move the BEP to a higher flow rate and flatten the head–capacity curve [19,20]. Another significant volute design parameter is the gap width. The reduction in the gap width has been shown to positively influence the efficiency of centrifugal pumps [18,19].

As can be inferred from the preceding paragraphs, there has been research focused on the application of unconventional designs to low-specific-speed hydraulics, investigations on studying the flow phenomenon inside the pump, parametric studies aimed at studying the sensitivity of performance features to different design variables, and other studies focused on coupling different optimization algorithms to numerical simulations to optimize the pump design for enhanced performance features. This paper explores the influence of the volute throat area and gap width on the performance characteristics of the low-specific-speed centrifugal pump by relating the change in performance features to the internal flow characteristics. Although studies have been conducted that examine the influence of these parameters on performance characteristics [18–20], this study focuses more on understanding the influence in terms of internal flow characteristics. To the knowledge of the authors, there is a lack of a comprehensive understanding of the impact of these parameters through the lens of internal flow physics at low specific speeds. Section 2 of the paper outlines the main dimensions of the pump and describes the numerical scheme used for the simulations. Section 3 presents the performance characteristics of the design defined in Section 2 (baseline design) and investigates the impact on these features as a result of the reduction in the volute throat area and gap width. Finally, Section 4 relates the impact of the volute geometry on the performance characteristics to the internal flow characteristics.

## 2. Design Parameters and Numerical Scheme

The dimensions defining the impeller were determined using velocity triangles and empirical relations suggested by Gulich [1]. These velocity triangles are derived from an idealized one-dimensional flow (streamline theory) and define the relation between the absolute and relative components of fluid velocity to the rotational speed of the impeller. These were used to determine the inlet and outlet angles of the impeller blades. The dimensions defining the meridional section of the impeller were established using empirical

relations based on experimental measurements of the performance of pumps of different sizes and specific speeds [1]. For the volute, the throat area and gap width were established using the constant velocity method suggested by Stepanoff [21]. The method is developed so that the circumferential fluid velocity remains constant across all cross-sections in the volute [21]. All these dimensions were established for a specific pumping task, which is defined by the chosen specific speed of the pump. The main dimensions of the impeller and volute are outlined in Table 1.

**Table 1.** Design parameters of the pump.

| | |
|---|---|
| Hub Diameter, $D_0$ | 35 mm |
| Inner Diameter, $D_1$ | 44 mm |
| Outer Diameter, $D_2$ | 48 mm |
| Outlet Width, $b$ | 18 mm |
| Number of Blades, $Z$ | 7 |
| Blade Inlet Angle, $\beta_1$ | 33° |
| Blade Outlet Angle, $\beta_2$ | 29° |
| Volute Throat Area | 1890 mm$^2$ |
| Volute Gap Width | 20 mm |

The pump designed using the dimensions outlined in Table 1 is referred to as the baseline design. The outlet width and outer diameter indicated in the table yield an area of 2714 mm$^2$ at the impeller–volute interface. The volute is designed as a spiral with its cross-sectional area increasing with angular displacement along the volute as measured from the cutwater. The volute throat is where its cross-sectional area is maximum and the flow rate is equal to the pump capacity under the design conditions. The pump is designed to deliver a head of 83 m at a flow rate of 0.02 m$^3$/s and a rotational speed of 1750 rpm. This yields a specific speed of 9, according to Equation (1).

The numerical simulations were performed using TCAE, which is a commercial simulation package built using OpenFoam. The numerical simulation involved the solution of the steady-state Reynolds-averaged Navier–Stokes (RANS) equations over the fluid domain. These steady-state equations are given as

$$\begin{aligned} \nabla \cdot \boldsymbol{u} &= 0 \\ \boldsymbol{u} \cdot (\nabla \boldsymbol{u}) &= v_{eff} \nabla^2 \boldsymbol{u} - \nabla p_k + \boldsymbol{g} \end{aligned} \tag{2}$$

where $\boldsymbol{u}$ is the velocity vector, $p_k$ is the kinematic pressure, $p_k = p/\rho$, and $v_{eff}$ is the effective kinematic viscosity. The effective kinematic viscosity is defined as the sum of fluid viscosity and computed eddy viscosity, which is defined based on a shear-stress transport (SST) $k-\omega$ turbulence model. The SST $k-\omega$ model is a combination of $k-\epsilon$ and $k-\omega$ models. The standard $k-\epsilon$ model is rendered undesirable due to its strong sensitivity to free-stream conditions [22]. This issue was resolved by Menter [23], who developed the SST $k-\omega$ model that combines the two turbulence models by means of a blending function so that it transforms into the $k-\epsilon$ model near the wall and the $k-\omega$ model in free-stream conditions.

The solver is based on a finite volume method (FVM). The governing equations were discretized, and a first-order numerical scheme was used. The pressure–velocity coupling required for the solution was performed using an SIMPLEC algorithm. Further details of the algorithm can be found in [24]. The residuals of all flow variables were monitored to verify that they were all reduced to less than $10^{-4}$ over the last 100 iterations to ensure the convergence and stability of the solution.

The fluid domain used for these computations was automatically discretized using the STL file of the designed pump. The mesh of the geometry was obtained using the `snappyHexmesh` utility of OpenFoam, which uses hexahedral-shaped cells to discretize the geometry. This involves the creation of a base mesh first that is defined in terms of the background mesh size. This is followed by local refinement near solid walls and

geometrical features such as leading or trailing edges. The result is a castellated mesh that is snapped onto the surface. Appropriate refinement levels were specified, with increased refinement levels applied for features such as the blade leading edge and the volute tongue. The grids obtained for the impeller and the volute for the coarse mesh case are shown in Figure 1.

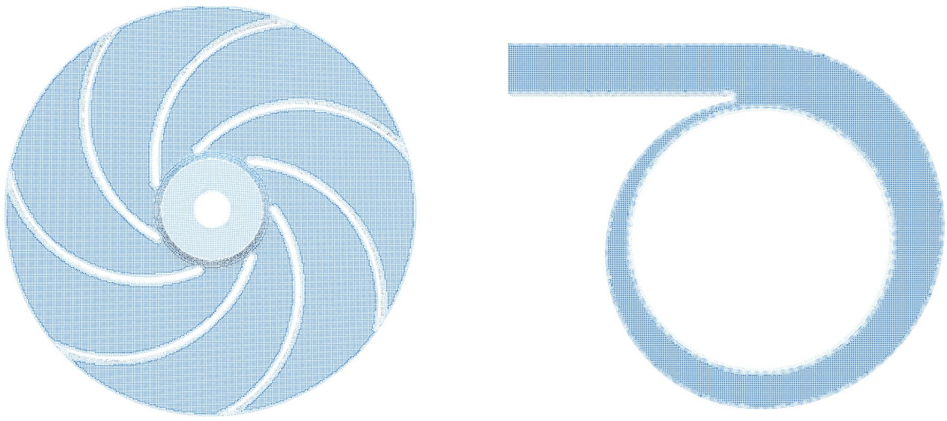

(**a**) (**b**)

**Figure 1.** Mesh grid used for numerical simulations for (**a**) impeller and (**b**) volute.

The interface between the impeller and volute was set as an arbitrary mesh interface (AMI), which maps the variable directly across the interface. The medium was selected as water at standard temperature and pressure (STP). The volumetric flow rate was specified as the boundary condition at the outlet, while the total pressure of 1 atm was used as the boundary condition at the inlet. The walls were treated with the no-slip boundary condition with standard wall functions, and appropriate refinement levels were added near the walls to adequately capture the effects of the boundary layer.

## 3. Mesh Independence Study and Performance Characteristics

The mesh independence study was performed using five different meshes, where the number of mesh elements was successively increased. The study was carried out by changing the background mesh size, with the same refinement levels used for the components. This was to ensure a uniformly refined mesh over the computational domain. The mesh independence was evaluated in terms of performance characteristics (head delivered, power required, and efficiency) at the design flow rate. The results of the study are shown in Figure 2.

The coarsest mesh was created with a background mesh size of 4.4 mm, while the second-coarsest mesh with a size of 3.2 mm. Subsequently, the mesh was successively refined by reducing the mesh size by 0.2 mm. As reflected in Figure 2, the performance characteristics do not change substantially as the background mesh size is reduced to 3.2 mm from 4.4 mm. However, further refinement by 0.2 mm results in a significant change in performance. As the mesh size is refined from 2.8 mm (2, 134, 208 cells) to 2.6 mm (2, 439, 305 cells), the head, efficiency, and power change by 0.26%, 0.26%, and 0.08%, respectively. With performance metrics changing by less than 0.5% after further refinement, the grid with a background mesh size of 2.8 mm was used for all simulations.

The first set of simulations was designed to investigate the impact of the reduction in the throat area on hydraulic performance. To this end, the performance features of the baseline design with the volute throat area reduced by 25%, referred to as design A, were compared to those of the baseline design. The area was reduced by only adjusting the height at the volute throat. Hence, the area defining the impeller–volute interface remained the same. The results obtained from the numerical simulations are shown in Figure 3.

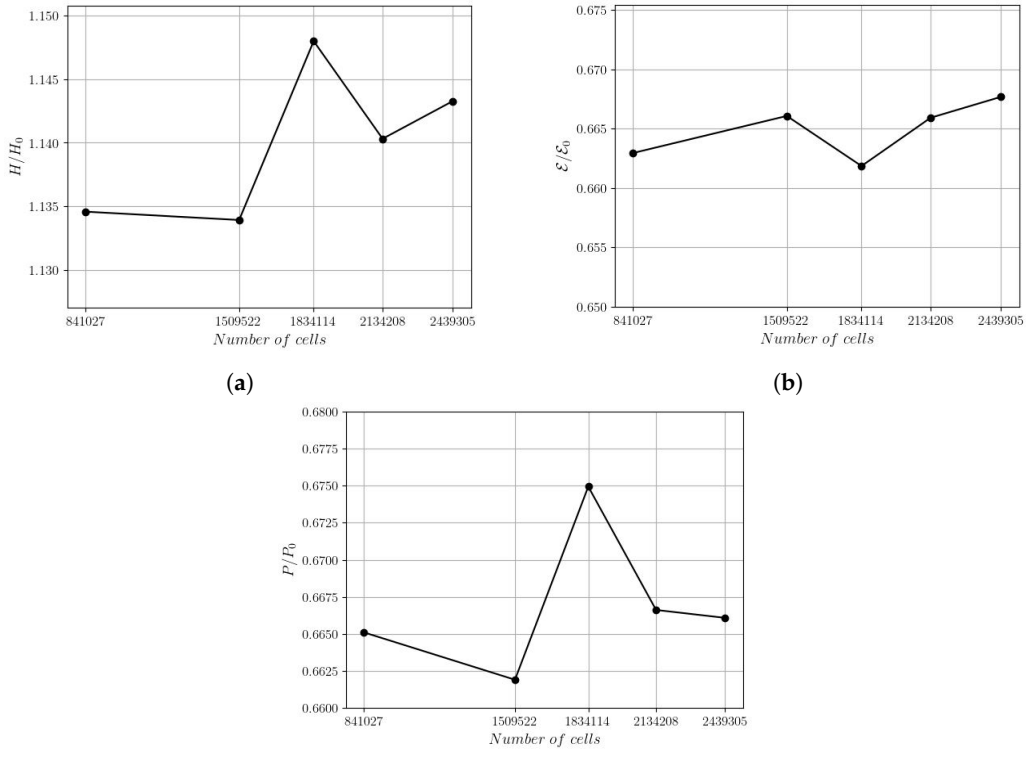


(**a**) (**b**)

(**c**)

**Figure 2.** Grid convergence study at the design flow rate for the normalized head (**a**), efficiency (**b**), and pressure (**c**).

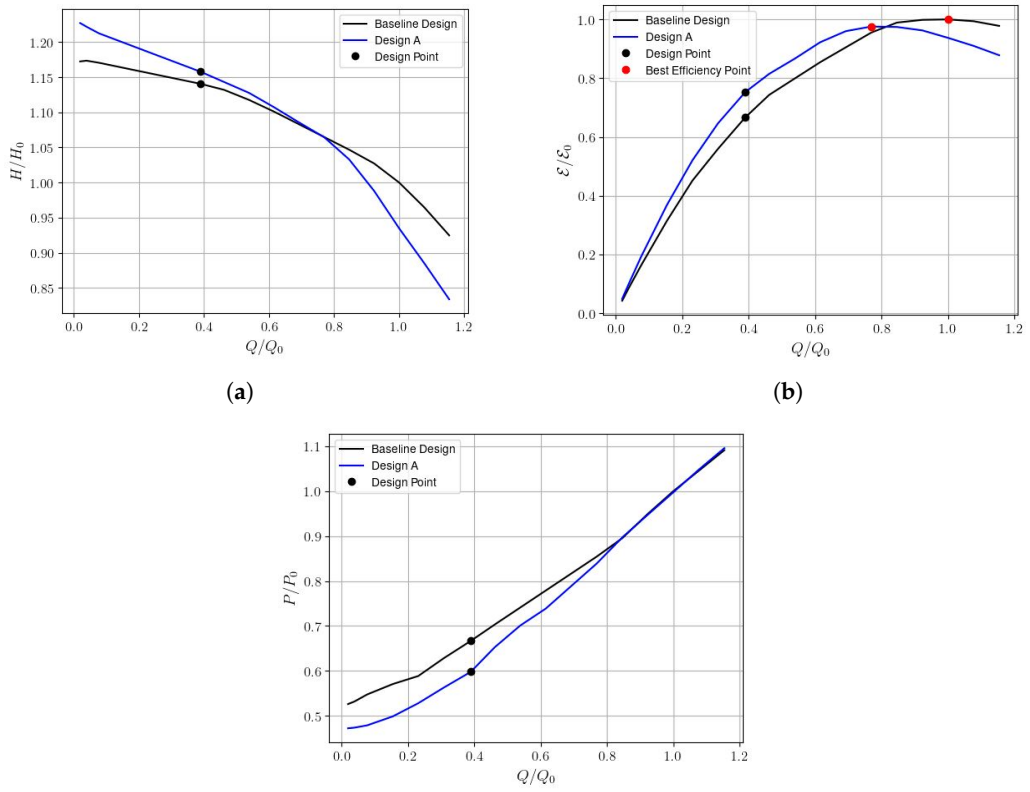


(**a**) (**b**)

(**c**)

**Figure 3.** Performance characteristics of baseline design in comparison to those of design A (baseline design with volute throat area reduced by 25%). The normalized head (**a**), efficiency (**b**), and pressure (**c**).

As can be inferred from Figure 3, the BEP of the baseline design is located at a much higher discharge rate than that corresponding to the design point. This phenomenon has also been realized through experimental investigations. Abramian and Howard [25] used LDV measurements to investigate the flow fields within the passage of a low-specific-speed impeller. Their results indicated that the BEP of the pump was located at 170% of the discharge rate corresponding to the design point. Figure 3 also shows that the reduction in the volute throat area resulted in the head–capacity curve becoming steeper and the BEP moving closer to the design point. In addition, it also led to reduced power consumption for flows of up to about $Q/Q_0 = 0.8$. These effects become more pronounced as the throat area is further reduced. This is evidenced in Figure 4, which shows the performance characteristics of the baseline design and design A compared to those of the baseline design with the throat area reduced by 50%, referred to as design B. Once again, the area was reduced by only adjusting the corresponding height, while the area defining the impeller–volute interface remained the same. The head–capacity curve becomes even steeper as the volute throat area is further reduced, with the BEP moving further toward the design point. The power consumption is also further reduced. Chabbanes et al. [20] used numerical simulations to show a flattened head–capacity curve and BEP displaced further to the right as the volute throat area was increased. The results of experimental investigations by Olimstad et al. [9] showed that a slight increase in the volute throat area of an extremely low-specific-speed pump resulted in higher head delivery under overload conditions, with negligible change at underload conditions. However, there is no comprehensive understanding of this change in performance characteristics in terms of flow physics. The impact of the volute gap width on the performance features was found to be not as pronounced as that observed for the case of the volute throat area.

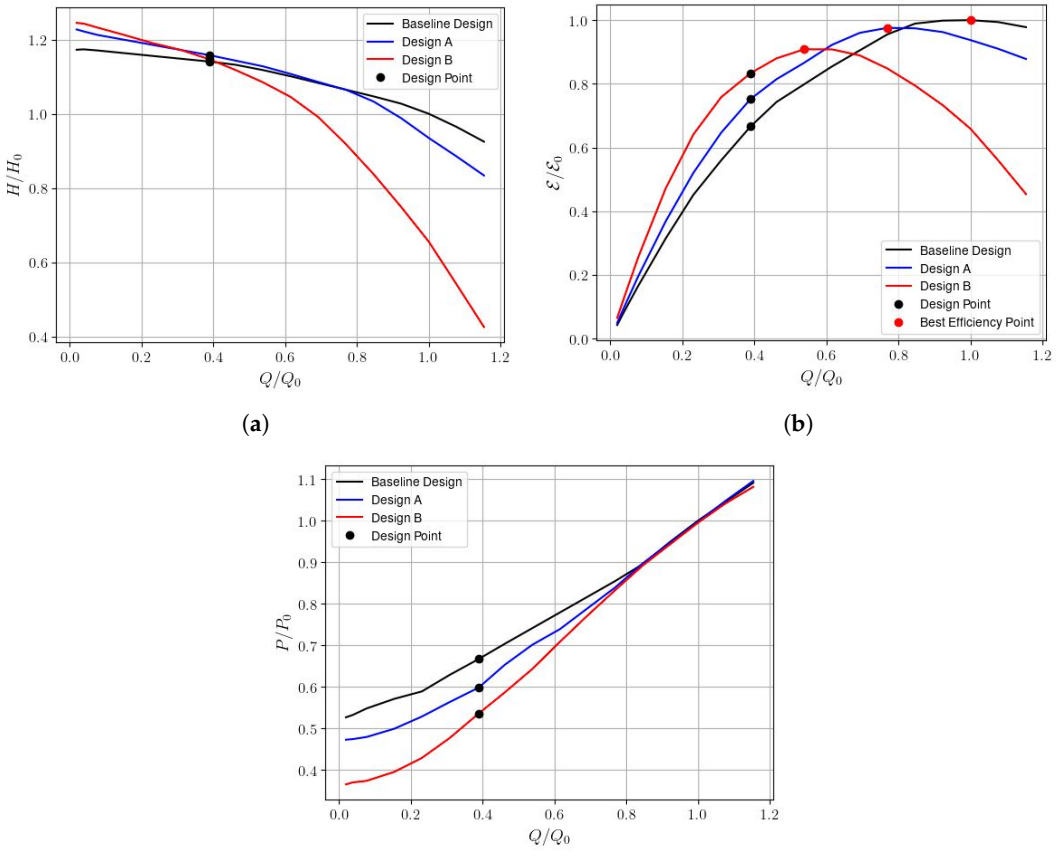


**Figure 4.** Performance characteristics, including the normalized head (**a**), efficiency (**b**), and pressure (**c**), of baseline design in comparison to those of design A and design B (baseline design with volute throat area reduced by 50%).

The impact of the volute gap width on performance characteristics was investigated by reducing the gap width of design B by 50% and examining the resulting change in performance characteristics. The reduction in the gap width by 25% did not produce any significant change in the performance characteristics. The performance characteristics of design B with the gap width reduced by 50%, referred to as design C, compared to those of design B are shown in Figure 5. There is a vertical translation of the head–capacity curve, with a slight improvement in efficiency at design load and overload conditions. There is also a slight increase in power requirements for underload conditions. Similar results have also been obtained through experimental investigations. The results of the experimental studies presented in [18,26] showed that the reduction in gap width resulted in higher head delivery across all the flow rates and an increase in efficiency, especially under design flow and overload conditions. However, these impacts have not been investigated at a fundamental level in terms of internal flow features. These effects and those resulting from throat area reduction can be understood well by a thorough investigation of the internal flow physics.

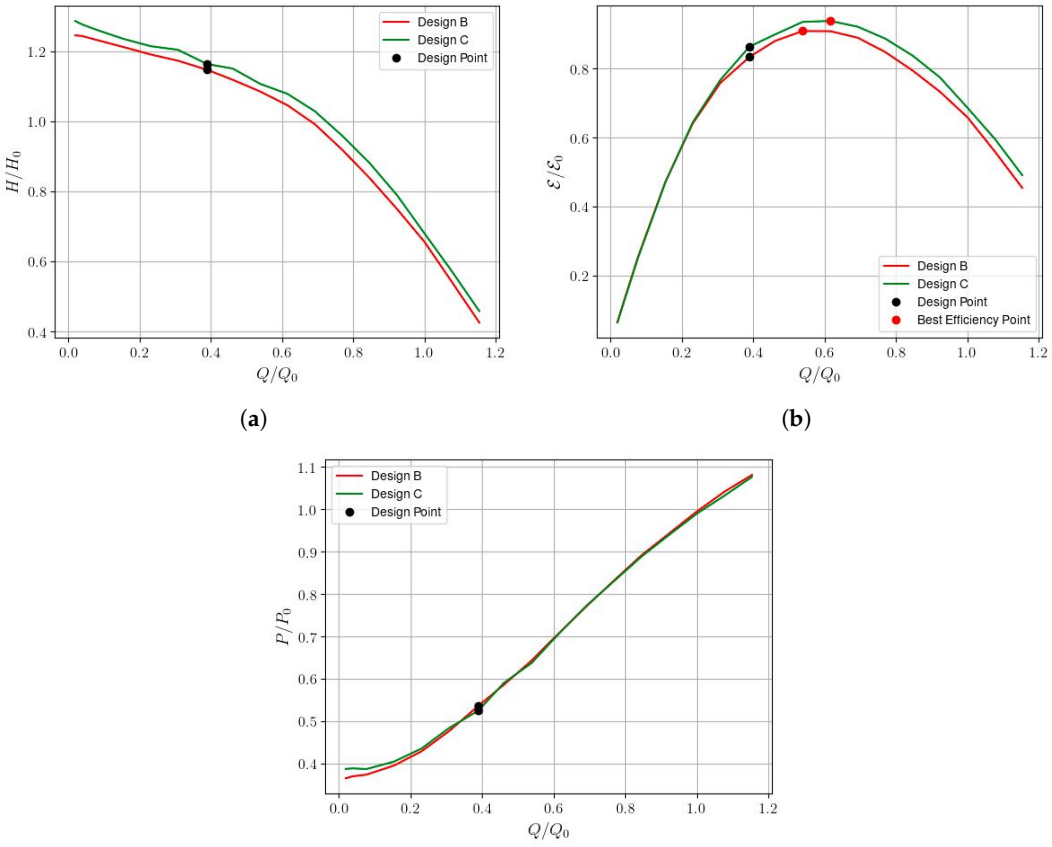


**Figure 5.** Performance characteristics, including the normalized head (**a**), efficiency (**b**), and pressure (**c**), of design B in comparison to those of design C (design B with volute gap width reduced by 50%).

## 4. Internal Flow Physics

As Figures 3 and 4 indicate, an improvement in efficiency resulting from the reduction in the volute throat area can be related to reduced power consumption. Power consumption is inversely related to hydraulic efficiency, so a reduction in power consumption would mean an increase in efficiency. Power, on the other hand, is a measure of the energy supplied (per unit time) to the shaft to rotate the impeller. This, in turn, is proportional to the pressure difference between the pressure and suction sides of the impeller blades. The greater the pressure difference, the greater the energy required to rotate the impeller, and hence, the greater the power consumption. This implies that the pressure between the two sides of

the blades is reduced as the volute throat area is reduced. This is further confirmed in Figure 6, which shows a comparison of the pressure distribution in the streamwise direction along the blade surface for a particular blade at midspan between baseline design and design B at multiple flow rates. Similar profiles of pressure distribution were obtained for other blades. It is evident that the pressure difference between the pressure and suction sides of the blade for the design with reduced throat area is less than that for the baseline design. This may suggest that the flow profile around the blade becomes more uniform as the volute throat area is reduced. This difference decreases toward the flow rate of $Q/Q_0 = 0.9$, which is consistent with Figure 4c, which shows that the power consumption of the two designs is essentially the same at $Q/Q_0 = 0.9$. In addition to reduced power consumption, the increase in head delivered with the reduction in throat area also results in improved efficiency.

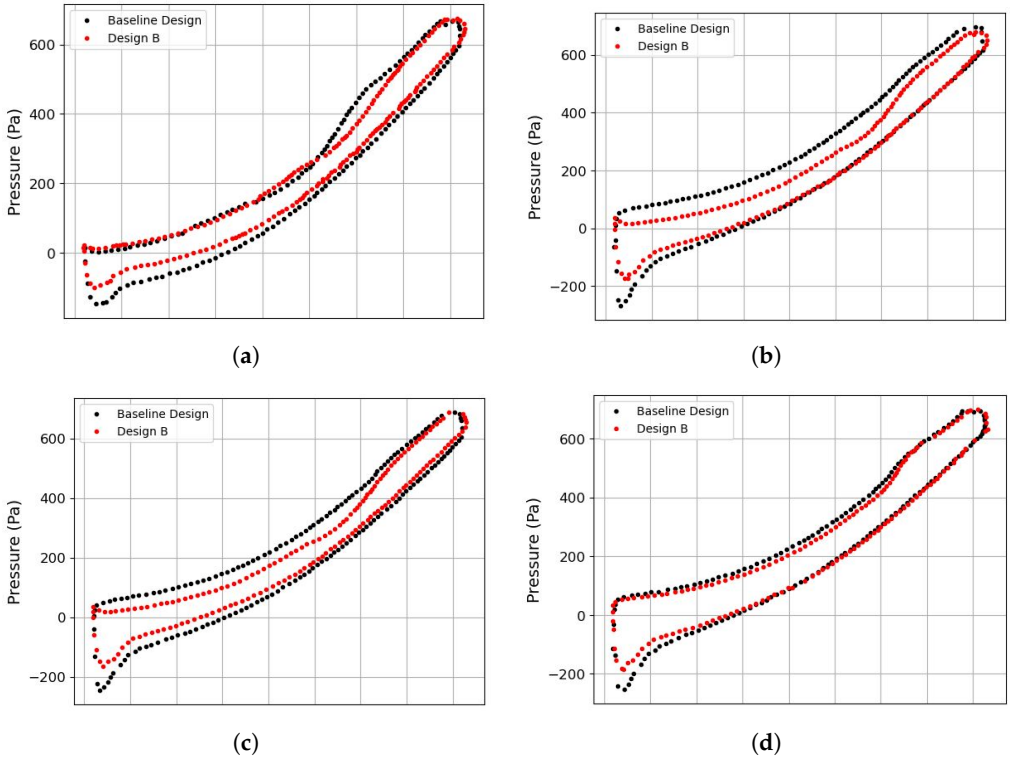


**Figure 6.** Distribution of gauge pressure over the pressure and suction sides of the blade at midspan in the streamwise direction at (**a**) $Q/Q_0 = 0.15$, (**b**) $Q/Q_0 = 0.4$, (**c**) $Q/Q_0 = 0.6$, and (**d**) $Q/Q_0 = 0.9$.

The head delivered is the result of the energy imparted by the impeller to the fluid and the losses incurred in the volute towards the outlet. From Figures 4 and 7, it is conclusive that the head delivered by the impeller of design B is greater than that delivered by the impeller of the baseline design for underload and design flow conditions. This indicates that the change in the flow profile in the impeller with throat area reduction described earlier also manifests itself in the form of an improved slip factor. The slip factor is a measure of the slip phenomenon, which refers to the flow streamlines being deviated towards the blade pressure side at the impeller outlet and resulting in dissipation losses. The lower the deviation, the greater the slip factor and the greater the head delivered by the impeller. The head delivered by the impeller, $H_{imp}$, can be related to the slip factor using the Euler equation for the head [21]. This is defined as

$$H_{imp} = \frac{u_2 c_{2u}}{g} \tag{3}$$

where $u_2$ is the impeller rotational speed at outlet, $c_{2u}$ is the magnitude of the tangential component of the fluid velocity at the outlet, and $g$ is the gravitational constant. The quantity $c_{2u}$ can be defined in terms of the slip factor, $\gamma$, using Equation (4) [1].

$$c_{2u} = u_2\left(\gamma - \frac{c_{2m}}{u_2 \tan \beta_{2B}}\right) \tag{4}$$

where $c_{2m}$ is the meridional component of the fluid velocity at the impeller outlet and is defined in terms of the flow rate and area at the impeller outlet through which the flow exits, while $\beta_{2B}$ is the blade outlet angle. Equation (4) can be substituted into Equation (3) to define the head delivered by the impeller in terms of the slip factor as

$$H = u_2^2\left(\gamma - \frac{c_{2m}}{u_2 \tan \beta_{2B}}\right) \tag{5}$$

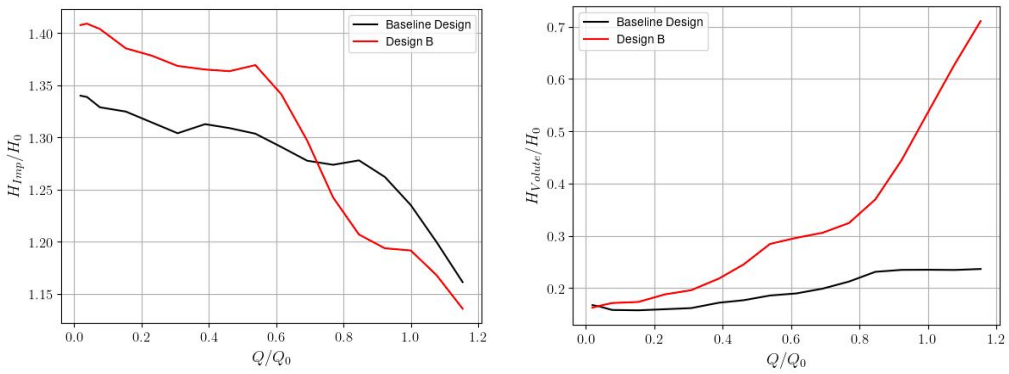


(**a**) (**b**)

**Figure 7.** (**a**) Head delivered by the impeller and (**b**) head loss incurred in volute of baseline deign in comparison to that for design B.

Equation (5) suggests that between the baseline design and design B, with all other factors that contribute to head delivery being the same, it is conclusive that a higher head delivered with a reduction in throat area is attributable to the improvement in the slip factor. Hence, the flow in the impeller becomes more blade-congruent as the throat area is reduced, in addition to the flow profile around the blade being more uniform. Both of these factors contribute to the improvement in the hydraulic performance of the pump. However, a counteracting effect occurs in the volute, where increased losses contribute to dramatically reducing the head output at overload conditions.

The reduced volute throat area results in increased viscous losses, which become more pronounced at overload conditions. This is conclusive from Figure 8, which shows the distribution of total mechanical energy in the midspan of the pump at a flow rate of $Q/Q_0 = 0.9$ for the baseline design and design B. It can be inferred that the throat area reduction yields increased dissipation losses near the tongue region of the volute, which contributes to reducing the overall head output. This also results in a significant increase in cavitation near the tongue region. This is evident in Figure 9, which shows the cavitation volume as a percentage of the total volume of the fluid domain for the two designs. There is negligible cavitation for the two designs up to a flow rate of approximately $Q/Q_0 = 0.75$, after which a marked increase in cavitation is observed for design B and it continues to rise. Similar results were obtained by Olimstad et al. [9], who showed that cavitation in the volute resulted in a steep decline in the head–capacity curve.

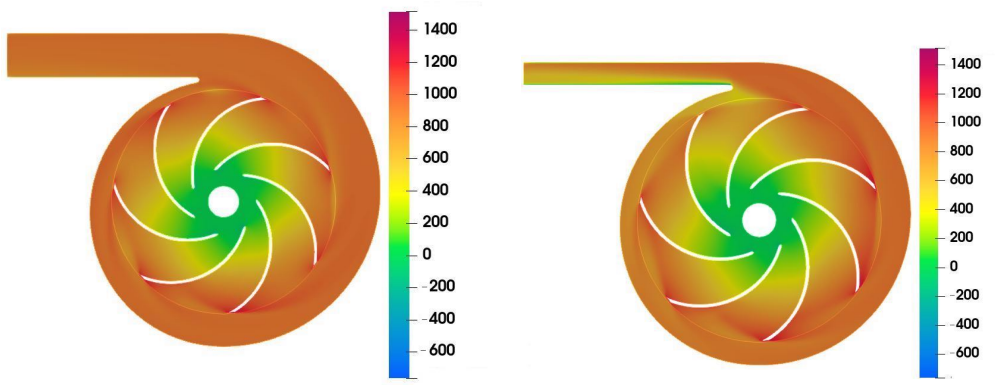


(**a**) (**b**)

**Figure 8.** Distribution of total mechanical energy at the midspan of the pump at the flow rate of $Q/Q_0 = 0.9$ for (**a**) baseline design and (**b**) design B. Note that the pressure part of the total energy is estimated as gauge pressure.

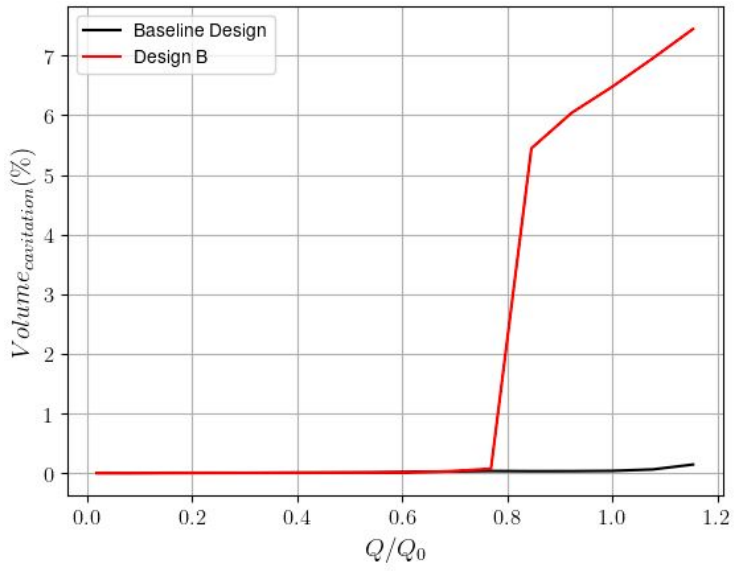


**Figure 9.** Cavitating volume for baseline design and design B.

A quantitative estimate of the pronounced viscous losses with a reduction in the throat area can be established from Figure 7b, which shows the head loss in the volute as a function of the flow rate for design B compared to that for the baseline design. It is obvious that the reduction in the throat area results in greater head losses, and the difference becomes more pronounced with the increase in the flow rate. The improved slip factor with reduction in the throat area results in a greater amount of head being delivered by the impeller, as shown in Figure 7a. This results in a greater head output at the outlet for underload and design flow conditions for design B, since there is no significant difference in volute head loss under these conditions. However, with increasing flow rate, the difference in viscous losses becomes significant, which dramatically reduces the head delivered. This is compounded by the slight decrease in the head delivered by the impeller under these conditions. This accounts for a steeper head–capacity curve for design B. The drop in head delivered also significantly impacts the hydraulic efficiency. While a higher head delivered and reduced power consumption result in improved efficiency for design B up to a flow rate of about $Q/Q_0 = 0.6$, dramatic head drop at higher flow rates leads to a sharp decrease in efficiency. This also results in the BEP moving closer to the design point. A similar analysis can be used to study the impact of the gap width on the performance features.

Figure 5 suggests that the reduction in the gap width results in a vertical translation of the head–capacity curve. The higher head also results in greater efficiency for design C. This effect can be well understood using Figure 10, which shows the head delivered by the impeller of design C compared to that delivered by the impeller of design B and the head loss incurred in the volute of the two designs. It is clear that the vertical translation in the head–capacity curve is attributable to greater head delivered by the impeller of design C, since there is negligible difference in the head loss incurred in the volute for all the flow rates between the two designs. As discussed earlier, according to Equation (5), with all the contributing factors to the delivered head being the same between the two designs, it is easier to conclude that the greater head delivered with the gap width reduction is attributable to the better slip factor. Hence, the gap width reduction changes the flow pattern in the impeller to be more blade-congruent, but has no major impact on the volute flow.

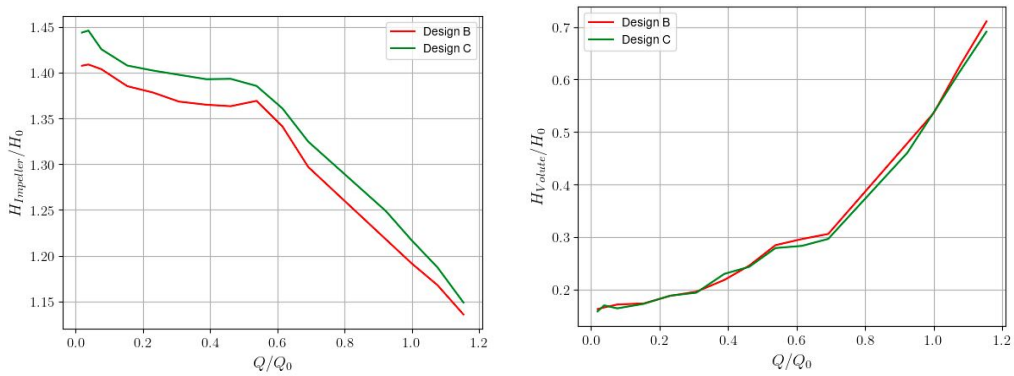


(**a**) (**b**)

**Figure 10.** (**a**) Head delivered by the impeller and (**b**) head loss incurred in volute of design B in comparison to that for design C.

## 5. Conclusions

This paper aims to relate the impact of the volute throat area and gap width on hydraulic performance to the resulting change in internal flow characteristics of a low-specific-speed centrifugal pump using numerical simulations. The results from numerical simulations reveal that the head–capacity curve becomes steeper and that the best efficiency point (BEP) becomes closer to the design point as the volute throat area is reduced. Efficiency also improves, especially at underload and design flow conditions. However, the efficiency decreases with higher flow rates. Examination of the internal flow field reveals that the flow profile around the blades becomes more uniform with reduction in throat area, which leads to reduced pressure difference between the pressure and suction sides of the blade. The reduced pressure difference, in turn, reduces the power consumed, leading to improved efficiency. The changed flow field in the impeller also manifests in the form of the slip factor being improved, i.e., the flow becomes more blade-congruent, which reduces the dissipation losses and leads to greater head delivered by the impeller. A counteracting effect occurs in volute with increased viscous losses near the tongue region with the reduction in the throat area. The difference in volute head loss is not substantial at underload and design flow conditions, which leads to increased head delivered at the outlet. Increased head output under these conditions leads to further improvements in hydraulic efficiency. However, the difference in volute head loss becomes more pronounced as the flow rate increases. This leads to a steep decline in head delivered at higher flow rates, which also leads to a dramatic decrease in efficiency under these conditions. The net effect is a steeper head–capacity curve, and a higher efficiency at the design point with the BEP moving closer to the design point.

The study on the impact of the volute gap width reveals that the gap width reduction leads to vertical translation of the head–capacity curve in the positive direction. This also improves the hydraulic efficiency at the design point and overload conditions. This was

found to be a consequence of the improved slip factor across all flow rates, which led to a higher head delivered by the impeller. There was essentially no difference in head loss incurred in the volute as the gap width was reduced. Therefore, the reduction in gap width yields favorable results for the hydraulic performance of low-specific-speed centrifugal pumps. However, there is a tendency of higher-pressure pulsations being developed as a result of a reduction in the gap width, especially near the tongue region of the volute. More studies are needed to investigate the change in unsteady flow characteristics with the reduction in volute gap width.

**Author Contributions:** Conceptualization: M.F.K., T.G. and N.G.; methodology: M.F.K. and T.G.; software: M.F.K. and T.G.; validation: M.F.K. and T.G.; formal analysis: M.F.K.; investigation: M.F.K. and T.G.; resources: J.-P.H.; data curation: M.F.K.; writing—original draft preparation: M.F.K.; writing—review and editing: M.F.K., T.G., N.G. and J.-P.H.; visualization: M.F.K. and T.G.; supervision: J.-P.H.; project administration: J.-P.H.; funding acquisition: J.-P.H. All authors have read and agreed to the published version of the manuscript.

**Funding:** The work was made possible due to funding received through Mitacs Accelerate program with Toyo Pumps North America Corp. as the partner organization. This research was enabled in part by support provided by SciNet and the Digital Research Alliance of Canada.

**Data Availability Statement:** The data that support the findings of this paper are available from the corresponding author, M.F.K., upon reasonable request.

**Acknowledgments:** Simulations were performed on the Niagara supercomputer at the SciNet HPC Consortium that is part of the Digital Research Alliance of Canada.

**Conflicts of Interest:** The authors T.G and N.G. were employed by Toyo Pumps North America Corp. This study received funding from MITACS Accelerate Program with Toyo Pumps as the partner organization. The partner organization had the following involvement with contextualize the problem space, provide guidance and supervision, interpret, and analyze the results, assistance in the writing and revision of the manuscript.

## Abbreviations

The following abbreviations are used in this manuscript:

| | |
|---|---|
| AMI | Arbitrary Mesh Interface |
| BEP | Best Efficiency Point |
| FVM | Finite Volume Method |
| RANS | Reynolds-Averaged Navier-Stokes |
| RPM | Revolutions Per Minute |
| SST | Shear-Stress Transport |
| STP | Standard Temperature and Pressure |

## References

1. Gülich, J.F. *Centrifugal Pumps*; Springer: Berlin/Heidelberg, Germany, 2008; Volume 2.
2. Jin, J.; Fan, Y.; Han, W.; Hu, J. Design and analysis on hydraulic model of the ultra-low specific-speed centrifugal pump. *Procedia Eng.* **2012**, *31*, 110–114. [CrossRef]
3. Choi, Y.D.; Kurokawa, J.; Matsui, J. Performance and Internal Flow Characteristics of a Very Low Specific Speed Centrifugal Pump. *J. Fluids Eng.* **2006**, *128*, 341–349. [CrossRef]
4. Barske, U. Development of some unconventional centrifugal pumps. *Proc. Inst. Mech. Eng.* **1960**, *174*, 437–461. [CrossRef]
5. Dahl, T. Centrifugal pump hydraulics for low specific speed applications. In *Proceedings of the 6th International Pump Users Symposium*; Turbomachinery Laboratories, Department of Mechanical Engineering: College Station, TX, USA, 1989.
6. Boitel, G.; Fedala, D.; Myon, N. Tip clearance effects on loads and performances of semi-open impeller centrifugal pumps at different specific speeds. In *Proceedings of the IOP Conference Series: Earth and Environmental Science*; IOP Publishing: Bristol, UK, 2016; Volume 49, p. 032013.
7. Satoh, H.; Uchida, K.; Cao, Y. Designing An Ultra-Low Specific Speed Centrifugal Pump. In Proceedings of the 22nd International Pump Users Symposium, Texas A&M University, Turbomachinery Laboratories, Houston, TX, USA, 28 February–3 March 2005.
8. Kagawa, S.; Kurokawa, J. New centrifugal pump in very low specific speed range. In Proceedings of the Fluids Engineering Division Summer Meeting, Hamamatsu, Japan, 24–29 July 2011; Volume 44403, pp. 89–96.

9. Olimstad, G.; Osvoll, M.; Finstad, P.H.E. Very Low Specific Speed Centrifugal Pump—Hydraulic Design and Physical Limitations. *J. Fluids Eng.* **2018**, *140*, 071403. [CrossRef]
10. Cui, B.; Wang, C.; Zhu, Z.; Jin, Y. Influence of blade outlet angle on performance of low-specific-speed centrifugal pump. *J. Therm. Sci.* **2013**, *22*, 117–122. [CrossRef]
11. Gao, B.; Zhang, N.; Li, Z.; Ni, D.; Yang, M. Influence of the blade trailing edge profile on the performance and unsteady pressure pulsations in a low specific speed centrifugal pump. *J. Fluids Eng.* **2016**, *138*, 051106. [CrossRef]
12. Balasubramanian, R.; Bradshaw, S.; Sabini, E. Influence of impeller leading edge profiles on cavitation and suction performance. In Proceedings of the Middle East Turbomachinery Symposia, Doha, Qatar, 17–20 March 2012; 2013 Proceedings; Turbomachinery Laboratory, Texas A&M Engineering Experiment Station: College Station, TX, USA, 2013.
13. Li, W. Effects of interface model on performance of a vortex pump in CFD simulations. *Int. J. Fluid Eng.* **2024**, *1*, 013901. [CrossRef]
14. Chen, B.; Yuan, X. Advanced Aerodynamic Optimization System for Turbomachinery. *J. Turbomach.* **2008**, *130*, 021005. [CrossRef]
15. An, Z.; Zhounian, L.; Peng, W.; Linlin, C.; Dazhuan, W. Multi-objective optimization of a low specific speed centrifugal pump using an evolutionary algorithm. *Eng. Optim.* **2016**, *48*, 1251–1274. [CrossRef]
16. De Donno, R.; Fracassi, A.; Ghidoni, A.; Morelli, A.; Noventa, G. Surrogate-based optimization of a centrifugal pump with volute casing for an automotive engine cooling system. *Appl. Sci.* **2021**, *11*, 11470. [CrossRef]
17. Lin, Y.; Li, L.; Yang, S.; Chen, X.; Li, X.; Zhu, Z. Performance prediction and optimization of hydrogenation feed pump based on particle swarm optimization–least squares support vector regression surrogate model. *Eng. Appl. Comput. Fluid Mech.* **2024**, *18*, 2315985. [CrossRef]
18. Kurokawa, J.; Matsumoto, K.; Matsui, J.; Imamura, H. Development of high efficiency volute pump of very low specific speed. In Proceedings of the 6th Asian International Conference on Fluid Machinery, Johor, Malaysia, 18–21 July 2001; pp. 250–255.
19. Yang, S.; Kong, F.; Chen, B. Research on pump volute design method using CFD. *Int. J. Rotating Mach.* **2011**, *2011*, 137860. [CrossRef]
20. Chabannes, L.; Štefan, D.; Rudolf, P. Volute throat area and wall modelling influence on the numerical performances of a very low specific speed pump. In *Proceedings of the IOP Conference Series: Earth and Environmental Science*; IOP Publishing: Bristol, UK, 2021; Volume 774, p. 012007.
21. Stepanoff, A.J. *Centrifugal and Axial Flow Pumps*; Wiley: Hoboken, NJ, USA, 1957.
22. Wilcox, D.C. Multiscale model for turbulent flows. *AIAA J.* **1988**, *26*, 1311–1320. [CrossRef]
23. Menter, F.R. Two-equation eddy-viscosity turbulence models for engineering applications. *AIAA J.* **1994**, *32*, 1598–1605. [CrossRef]
24. Versteeg, H.K.; Malalasekera, W. *An Introduction to Computational Fluid Dynamics: The Finite Volume Method*; Pearson Education: England, UK, 2007; pp. 49–78.
25. Abramian, M.; Howard, J. Experimental Investigation of the Steady and Unsteady Relative Flow in a Model Centrifugal Impeller Passage. *J. Turbomach.* **1994**, *116*, 269–279. [CrossRef]
26. Kurokawa, J.; Matsumoto, K.; Matsui, J.; Kitahora, T. Performances of centrifugal pumps of very low specific speed. In *Hydraulic Machinery and Cavitation, Proceedings of the XIX IAHR Symposium: Section on Hydraulic Machinery and Cavitation, Singapore, 9–11 September 1998*; International Association of Hydraulic Research (IAHR): Madrid, Spain, 1999; Volume 2.